

Rapid circular microfluidic mixer utilizing unbalanced driving force

Che-Hsin Lin · Chien-Hsiung Tsai · Chih-Wen Pan · Lung-Ming Fu

Published online: 11 November 2006
© Springer Science + Business Media, LLC 2007

Abstract This paper proposes a novel rapid circular microfluidic mixer for micro-total-analysis-systems (μ -TAS) applications in which an unbalanced driving force is used to mix fluids in a circular chamber at low Reynolds numbers (Re). The microfluidic mixer has a three-layered structure and is fabricated on low-cost glass slides using a simple and reliable fabrication process. Using hydrodynamic pumps, fluids are driven from two inlet ports into a circular mixing chamber. Each inlet port separates into two separate channels, which are then attached to opposite sides of the 3-dimensional (3-D) circular mixing chamber. The unequal lengths of these inlet channels generate an unbalanced driving force, which enhances the mixing effect in the mixing chamber. Numerical simulations are performed to predict the fluid phenomena in the mixing chamber and to estimate the mixing performance under various Reynolds number conditions. The numerical results are verified by performing flow visualization experiments. A good agreement is found between the two sets of results. The numerical and experimental results reveal that the mixing performance can reach 91%

within a mixing chamber of 1 mm diameter at a Reynolds number of $Re = 3$. Additionally, the results confirm that the unbalanced driving force produces a flow rotation in the circular mixer at low Reynolds numbers, which significantly enhances the mixing performance. The novel micromixing method presented in this study provides a simple solution for mixing problems in Lab-on-a-chip systems.

Keywords Circular microfluidic mixer · Low Reynolds numbers · Lab-on-a-chip

1 Introduction

Microfluidic mixers have attracted considerable attention for various applications in the fields of micro-total-analysis-systems (μ -TAS), Lab-on-a-Chip systems, and chemical process technology (Tabuchi et al., 2004; Fu et al., 2004; Kamei et al., 2005; Xiang et al., 2005; Xuan and Li, 2005; Wang et al., 2006; Wei et al., 2006). Therefore, developing a thorough understanding of the mechanisms governing electrokinetic manipulations, particularly those associated with discrete micromixers, is essential if microfluidic systems designs are to be optimized. Most microfluidic mixing systems are limited to the low Reynolds number regime, and therefore species mixing occurs predominantly through diffusion effects rather than through the convection or turbulence mechanisms associated with higher Reynolds numbers. Thus, microfluidic devices which require a mixing operation typically bring the individual fluid streams together within a single channel and rely on diffusive effects to mix the two samples (Liu et al., 2000). However, diffusive mixing tends to be slow and therefore requires a relatively long mixing channel to obtain a satisfactory mixing performance.

C.-H. Lin
Department of Mechanical and Electro-Mechanical Engineering,
National Sun Yat-sen University,
Kaohsiung, Taiwan, 804

C.-H. Tsai (✉) · C.-W. Pan
Department of Vehicle Engineering, National Pingtung University
of Science and Technology,
Pingtung, Taiwan, 912
e-mail: chtsai@mail.npust.edu.tw

L.-M. Fu (✉)
Department of Materials Engineering, National Pingtung
University of Science and Technology,
Pingtung, Taiwan, 912
e-mail: loudyfu@mail.npust.edu.tw

In general, microfluidic mixers can be categorized as either active microfluidic mixers or passive microfluidic mixers. Active microfluidic mixers generally achieve mixing by applying an external field to generate a flow disturbance. Accordingly, active microfluidic mixers can be further categorized in terms of the type of external disturbance effect they apply, e.g. temperature, acoustic/ultrasonic, pressure, actuator, electrokinetic, magneto-hydrodynamic, electro-hydrodynamic, or dielectrophoretic. However, the integrated components required to generate the external field complicate the structure, and hence the fabrication procedure, of these active microfluidic mixers. The earliest active microfluidic mixers utilized disturbances of a pressure field to generate a mixing effect. Tang et al. (2002) and Fujii et al. (2003) used an integrated planar micropump to sequentially drive and stop the flow in the mixing channel in order to partition the mixed liquids into serial segments and to render the mixing process independent of convection. Glasgow et al. (2004) and Coleman and Sinton (2005) performed numerical and experimental investigations into a simple T-mixer using a pulsed side flow to perform mixing at a low Reynolds number (0.3). The structure of a microfluidic mixer based on electro-hydrodynamic disturbances is similar to that of the mixer presented by Niu and Lee (2003) and Dodge et al. (2004) in which an actuator system was used to produce a series of oscillating periodic flows to enhance the mixing efficiency.

Lin et al. (2004) and Fu et al. (2005) presented active T-shaped and double-T-shaped microfluidic mixers utilizing a low-frequency switching electroosmotic flow. These mixers employed a single electrokinetic driving force to drive the sample fluids and produce a periodic switching frequency. This approach has the advantage that no other form of external driving force is required to induce perturbations in the flow field. Yang et al. (2000) proposed an active microfluidic mixer using lead-zirconate-titanate (PZT)-generated ultrasonic vibrations to enhance the mixing performance. Liu et al. (2003) carried out mixing by exploiting the acoustic streaming effect induced around an air bubble by an integrated PZT actuator. Yaralioglu et al. (2004) also utilized acoustic streaming to disturb the flow in a conventional Y-shaped microfluidic mixer. In a non-related study, Mao et al. (2002) established a linear temperature gradient across a number of parallel channels. Although this technique was originally proposed as a means of investigating the temperature dependence of fluorescent dyes, it also has potential for micromixing applications.

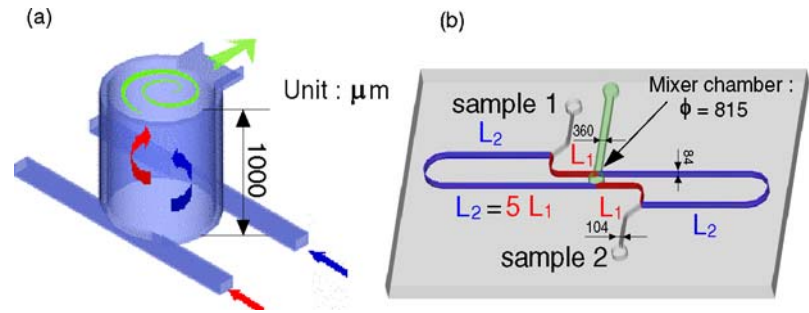
In contrast to the active micromixers discussed above, passive microfluidic mixers do not require an external energy source, but carry out the mixing process using only diffusion or chaotic advection mechanisms. Passive microfluidic mixers can be categorized on the basis of their arrangement of the mixed phases, i.e. parallel flow, serial lamination, hy-

drodynamic focusing, flow separation, chaotic advection, or split and recombined flows. The parallel flow arrangement splits the inlet flows into n sub-flows and species mixing is achieved via diffusion. The basic design of micromixers of this type involves a long microchannel with two inlet streams. Typical designs include the T-shaped microfluidic mixer and the Y-shaped microfluidic mixer (Wu et al. 2004); (Wong et al., 2004). Hydrodynamic focusing techniques were first developed by Knight et al. (1998) to perform the ultra-fast mixing (in the millisecond range) of one fluid lamella. In hydrodynamic focusing designs, the micromixer is equipped with three inlets; a central inlet for the sample flow and two outer inlets for the supply of solvent streams to sheath the sample flow. The latest generation of mixing devices using extreme hydrodynamic focusing is the SuperFocus mixer proposed by Löb et al. (2004) and Hardt and Schönfeld (2003), which features a multi-lamination pattern in the focusing zone.

Microfluidic mixers based on chaotic advection can be derived from the microscale design with three-dimensionally twisted conduits. Liu et al. (2000), Chen and Meiners (2004) and Park et al. (2004) fabricated passive microfluidic mixers with three-dimensional serpentine microchannels on silicon and glass substrates, respectively. It is known that the mixing performance of micromixers is enhanced at high Reynolds numbers, which suggests that chaotic advection occurs predominantly at higher Reynolds numbers (i.e. $Re = 25-70$). Hong et al. (2004) demonstrated an in-plane micromixer with a two-dimensional modified Tesla structure. It was shown that the Coanda effect in this structure prompted chaotic advection and significantly improved the mixing performance in flows with Reynolds numbers of $Re > 5$. Various other forms of three-dimensional passive microfluidic mixer structures have also been proposed (Kim et al., 2004a, b; Chung et al., 2004; Lin et al., 2005). For example, several studies have indicated that grooves on the channel wall can generate chaotic advection and therefore enhance the mixing efficiency (Johnson et al., 2002; Stroock et al., 2002; Ferrigno et al., 2004; Liu et al., 2004; Kang and Kwon 2004). Johnson et al. (2002) were among the first researchers to investigate this phenomenon. In their study, grooves were ablated on the base of the microchannel using a laser and it was shown that the mixing performance attained a level of 99% at a cross-section located 6.9 cm downstream from the T-junction. Stroock et al. (2002) also investigated this effect and published their results in *Science*.

It has been reported that electroosmotic flow microfluidic mixers featuring only a patterned surface modification (Erickson and Li, 2002; Biddiss et al., 2004; Chang and Yang 2004) can also enhance mixing. The use of heterogeneous surface charge distributions along the microchannel walls has also been explored as a means of inducing separation vortices to enhance the mixing efficiency. He et al. (2001) and

Fig. 1 Schematic illustration of circular micro-chamber mixer geometry



Burke and Regnier 2003) performed stopped-flow enzyme assays using microfabricated static mixers and demonstrated that these devices are capable of providing a similar level of performance to that obtained from an external mixing device. In addition to the devices presented above, researchers have also proposed the use of zigzag (Mengeaud et al., 2002; Kakuta et al., 2001) and curved-square micromixing devices (Schönfeld and Hardt 2004; Jiang et al., 2004).

Most passive micromixers are suitable for mixing two sample fluids in complex geometry microfluidic channels, afterwards they will be mixed in the mixing chamber. The present study fabricates a novel passive microfluidic mixer on low-cost glass slides using a simple and reliable fabrication process. In the proposed approach, each sample fluid is supplied to the circular mixing chamber via two channels of unequal length, as shown in Fig. 1. The resulting unbalanced driving force generates 3-D vortices in the mixing chamber. It is shown that these vortices enhance the mixing performance at low Reynolds numbers.

2 Microchip fabrication

In order to generate a stable flow during the experimental tests, the two fluid channels connecting each inlet port to the circular mixing chamber are designed with different lengths such that the flow resistances in the channels are unequal. Therefore, a multilayered microfluidic chip is required to achieve the necessary channel crossovers for different kind of samples. In addition, since the proposed microchip is powered by a syringe pump, high pressures will be generated in the microfluidic channels during the mixing experiments. Therefore, the microchip assembly must have a high mechanical strength and a good bonding strength between the various substrates. Accordingly, the present micromixer is fabricated on low-cost soda-lime plates rather than on plastic or silicon based substrates (Fu and Lin, 2003,2003a, Fu and Lin 2004). Figure 2 presents a simplified schematic illustration of the current fabrication process. Initially, microscope slides were cleaned using a boiling piranha solution and then patterned with positive photoresist (AZ 4620, Clariant Corp., USA) by a standard photolithography procedure (Fig.

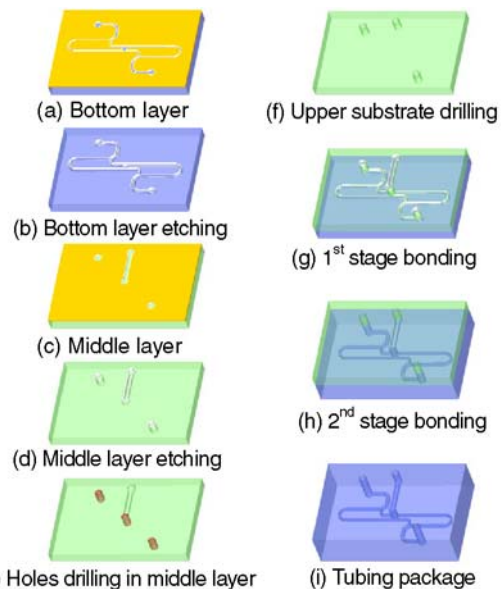


Fig. 2 Schematic representation of fabrication process employed for current micromixer

2(a)). The patterned glass substrates were then immersed in an ultrasonically agitated BOE bath for 40 min to generate microchannels of depth 36 μm (Fig. 2(b)). The second layer of the multilayered microchip was fabricated using the same photolithography and etching processes (Figs. 2(c) and (d)). Fluid via-holes and the mixing chamber were then drilled in the second layer using a diamond drill-bit (Fig. 2(e)). A third glass substrate was then drilled with through holes to form the sample inlets (Fig. 2(f)). The three substrates were cleaned in a boiling piranha solution and then bonded using a two-stage fusion bonding process designed to achieve a high bonding strength. In the bonding process, the upper and middle glass substrates were bonded in a sintering oven for 20 min at a temperature of 580°C (Fig. 2(g)). In the second stage of the bonding process, the same thermal treatment conditions were applied to bond the lower substrate and the previously sealed structure (Fig. 2(h)). Finally, Teflon tubing with an outer diameter of 1.5 mm and an inner diameter of 500 μm was packaged using epoxy glue to form the connections between the microchip device and the syringes holding the two mixing samples.

Fig. 3 (a) Photographic image of assembled micromixer. Note that channels are filled with red dye to enhance observation. (b) SEM image of mixing chamber

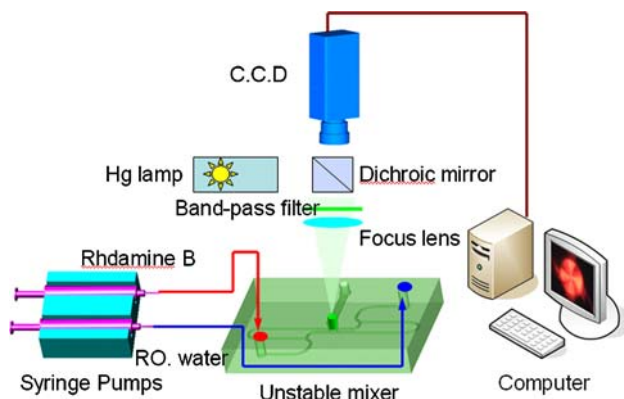
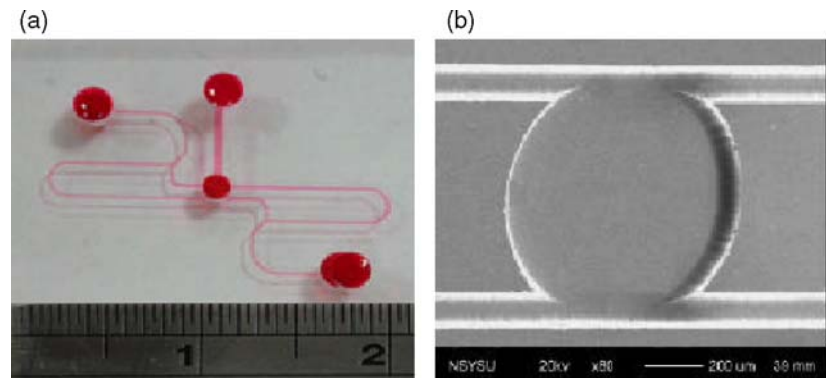


Fig. 4 Schematic illustration of experimental setup

Figure 3(a) presents a photo of the assembled microfluidic mixer. The fabricated chip has dimensions of $30 \text{ mm} \times 26 \text{ mm}$ (width \times length) and the mixing chamber is $815 \mu\text{m}$ in diameter and 1 mm in height. The sample outlet channel is orientated perpendicularly to the mixing chamber between the upper and middle substrates and has a diameter of $360 \mu\text{m}$ and a depth of $30 \mu\text{m}$. The SEM image of the circular mixing chamber shown in Fig. 3(b) shows that the chamber has a very sharp geometry and a smooth etched surface. Figure 4 presents a schematic illustration of the experimental setup used to test the proposed unbalanced driving force microfluidic mixer. In this setup, high precision syringe pumps (KDS-200, KD scientific, USA) are used to generate the necessary hydrodynamic driving forces. The two mixing fluids are DI water and a solution with 10^{-6} M Rhodamine B fluorescence dye or containing blue dye, respectively. The experimental tests were performed under a fluorescence microscope (E-400, Nikon, Japan) using a mercury lamp module for fluorescein excitation. A CCD module (DXC-190, Sony, Japan) with a high-speed image acquisition interface (DVD PKB, V-gear, Taiwan) was used to acquire the optical images. The captured images were then analyzed using digital imaging techniques to evaluate the mixing performance.

3 Mathematical framework

In general, comprehensive computational fluid dynamics simulations are usually conducted before physical models are built and tested because these simulations enable all of the system parameters to be varied over a wide range of values and permit simultaneous and instantaneous data collection throughout the model. Numerical simulation is an important technique in optimizing micro-mixer designs and enables a reliable interpretation of the experimental results.

The numerical results presented for the current microfluidic mixer are based on the solution of the incompressible Navier-Stokes equations, i.e.

$$\nabla_i u_i = 0, \quad (1)$$

$$\rho \frac{\partial u_i}{\partial t} + \rho (u_j \cdot \nabla_j) u_i = -\nabla_i p + \mu \nabla^2 u_i, \quad (2)$$

and on the convection-diffusion equation for a concentration distribution, i.e.

$$\frac{\partial C}{\partial t} + (u_i \cdot \nabla_i) C = D \nabla^2 C, \quad (3)$$

where u_i denotes the fluid velocity, ρ the density, μ the viscosity, D the binary diffusion coefficient, p the pressure, and C the concentration. In the present simulations, ρ , μ and D are assigned values of 1000 kg/m^3 , $0.001 \text{ kg/m} \cdot \text{sec}$ and $10^{-7} \text{ m}^2/\text{sec}$, respectively.

In this study, the governing equations were cast into a set of finite difference equations by the third order QUICK scheme (Leonard, 1987). The technique employed here was the finite-volume method. Note that the adoption of the QUICK scheme is consistent with the recommendations of Hardt and Schönfeld (2003) aimed at minimizing the numerical diffusion. The SIMPLEC algorithm (van Doormal

and Raithby 1984) was then used to solve the resulting difference equations for the pressure-velocity coupling in the Navier-Stokes equations.

As shown in Fig. 1, the circular micro-chamber contains four inlet microchannels and one outlet microchannel. In the present simulations, the inlet velocity of the four inlets was set to 0.87–30 cm/sec, corresponding to Reynolds numbers in the range 0.5–17.1. In this study, the Reynolds number is defined as,

$$\text{Re} = \frac{\rho u D_h}{\mu},$$

where D_h is the hydraulic diameter of the inlet microchannels. In the simulations, the fully developed condition was applied in the outlet microchannel, a no-slip boundary condition was imposed on the micro-chamber walls, and it was assumed that the sample concentration had zero flux.

In order to ensure a good resolution of the numerical results, the computational domain was discretized with structural hexahedral meshes, with most of the cells having equal sides of length 5 μm . The computational domain contained approximately 800,000 cells.

4 Results and discussion

4.1 Irrotational flow

The present numerical simulation results provide a clear understanding of the physical phenomena which take place in the unbalanced driving force circular microfluidic mixer and enable a rapid and accurate estimation of the mixing performance. Figure 5 presents the 3-D streamline distributions in the mixing chamber at a Reynolds number of $\text{Re} = 1$. The

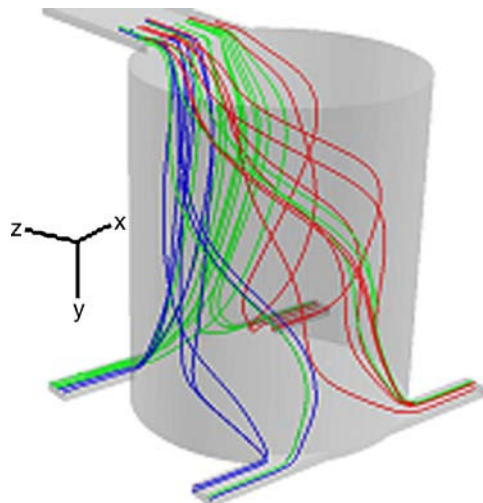


Fig. 5 3-D streamline distributions in circular micro-chamber at $\text{Re} = 1$ (a) Side view and (b) top view

Reynolds number can be defined as the ratio of the inertia forces to the viscous forces. Fluid flows with “sufficiently large” inertia forces (i.e. a sufficiently high Reynolds number) generally produce a self-rotation effect in the circular micro-chamber. However, flows in which the inertia forces are “small” compared with the viscous forces are characteristically laminar in nature (i.e. irrotational flows). In flows with a Reynolds number of $\text{Re} = 1$, the inertia forces in the circular micro-chamber are smaller than the viscous forces. Therefore, as shown in Fig. 5, the unbalanced driving force is insufficient to produce a flow rotation and the streamlines flow directly from the inlet to the outlet of the circular micro-chamber.

Figure 6 shows the numerical simulation results obtained for the species concentration distribution at different cross-sections of the circular micro-chamber for a Reynolds number of $\text{Re} = 1$. As discussed above, a flow rotation is not induced in the circular micro-chamber at this particular value of the Reynolds number. Figures 6(a)–(c) show that the species concentration distribution has two very distinct areas. Therefore, the mixing performance is dominated by the diffusion of the two samples and therefore this low Reynolds number flow fails to provide an effective species mixing. Figure 7 presents the species concentration contours at a cross-section located 100 μm downstream from the outlet of the mixing chamber and plots the normalized concentration intensity at different heights of the sample outlet channel for a Reynolds number of $\text{Re} = 1$. In this figure, the normalized concentration values of the two samples are 1 and 0, respectively, and therefore a value of 0.5 indicates that the two samples are fully mixed. It is obvious that the normalized concentration profiles in Fig. 7 deviate significantly from the fully-mixed condition. To quantify the degree of mixing in the outlet channel, the present study adopts the following mixing ratio parameter (Erickson and Li 2002),

$$\sigma = \left(1 - \frac{\int_A |C - C_\infty| dA}{\int_A |C_0 - C_\infty| dA} \right) \times 100\% \quad (4)$$

where C is the species concentration profile across the width of the mixing channel, and C_0 and C_∞ are the species concentrations in the completely unmixed (0 or 1) and completely mixed states (0.5), respectively. Analyzing the results of Fig. 7, it is found that a mixing ratio of 51.22% is obtained for a Reynolds number of $\text{Re} = 1$. This result confirms that irrotational flow fields in the circular micro-chamber yield a poor mixing of the two samples.

4.2 Rotational flow

Most passive microfluidic mixers adopt complex geometry microchannels to increase the contact area and contact time

Fig. 6 Numerical simulation results for species concentration distributions at different cross-sections of circular micro-chamber at $Re = 1$, (a) $Z = 20 \mu\text{m}$, (b) $Z = 460 \mu\text{m}$, and (c) $Z = 950 \mu\text{m}$

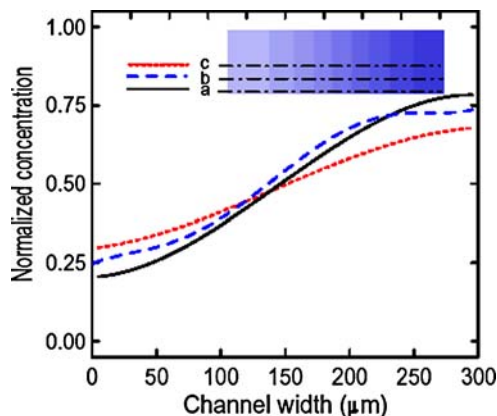
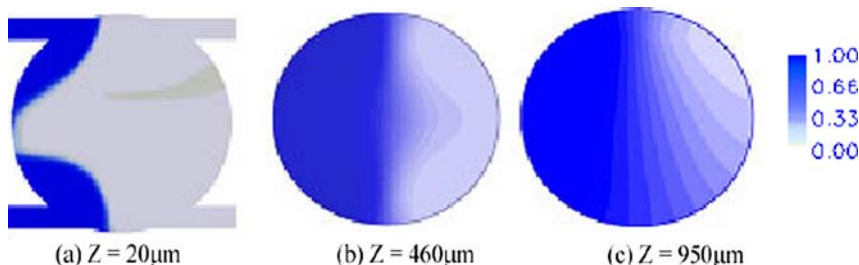


Fig. 7 Species concentration contours at cross-section located $100 \mu\text{m}$ downstream from outlet and normalized concentration intensity at different heights at $Re = 1$

of the sample fluids in order to enhance the mixing performance. In these designs, mixing is obtained by diffusive effects only and hence the mixing channel must have an extended length in order to achieve a satisfactory mixing result. However, this study aims to enhance the mixing performance at low Reynolds numbers by utilizing an unbalanced driving force to induce a 3-D vortex in the circular micro-chamber. In the current circular micro-chamber, the critical value of the Reynolds number, i.e. the value of the Reynolds number at which irrotational flow transits to rotational flow, is found to be 1.85. Therefore, an acceptable mixing performance is obtained by establishing flows with Reynolds numbers of 1.85 or higher.

Figure 8 illustrates the 3-D streamline distribution in the circular micro-chamber at a Reynolds number of $Re = 3$. As this Reynolds number, the inertia forces are “sufficiently larger” than the viscous forces and a flow rotation is induced.

Fig. 9 Numerical simulation results for species concentration distributions at different cross-sections in circular micro-chamber at $Re = 3$, (a) $Z = 20 \mu\text{m}$, (b) $Z = 460 \mu\text{m}$, and (c) $Z = 980 \mu\text{m}$

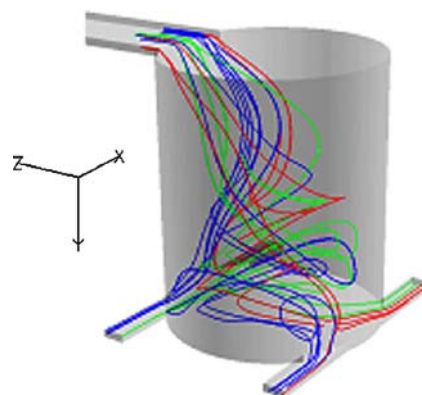
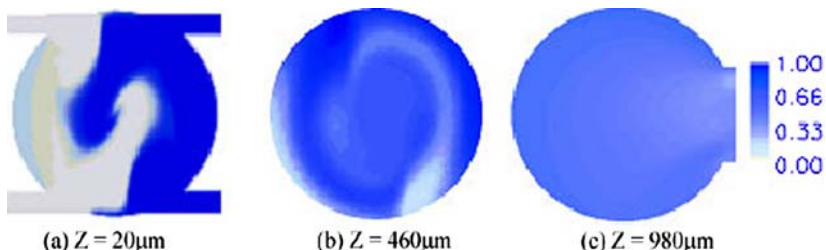


Fig. 8 3-D streamline distributions in circular micro-chamber at $Re = 3$

The streamlines in Fig. 8 reveal a rotation phenomenon and show the presence of an induced 3-D vortex in the circular micro-chamber. Figure 9 shows the numerical simulation results for the species concentration distributions at different cross-sections of the circular micro-chamber at a Reynolds number of $Re = 3$. When the samples are initially loaded into the circular micro-chamber, the species concentration distribution exhibits two very distinct regions. However, the unbalanced driving force is sufficient to subsequently establish rotational flow in the micro-chamber, and hence a 3-D vortex is formed. The spiral distribution pattern resulting from this rotational flow field is clearly evident in Fig. 9.

Figure 10 shows the species concentration contours at a cross-section located $100 \mu\text{m}$ downstream from the outlet of the micro-chamber at a Reynolds number of $Re = 3$ and plots the normalized concentration intensity at different channel heights. The results show that the normalized concentration intensity profiles are very close to 0.5 (i.e. a

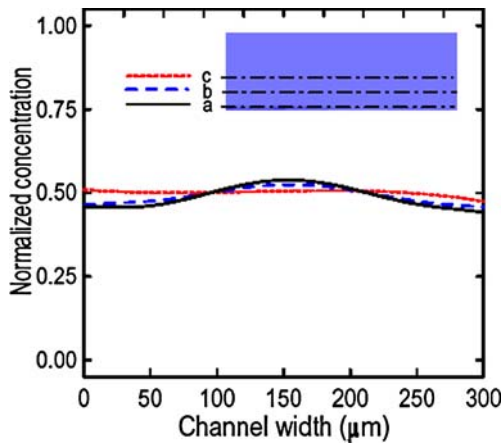


Fig. 10 Species concentration contours at cross-section located 100 μm downstream from outlet and normalized concentration intensity at different heights at $\text{Re} = 3$

fully-mixed condition) across the channel width. The mixing ratio in the outlet region is found to be 91.23%. Comparing Fig. 10 ($\text{Re} = 3$) with Fig. 7 ($\text{Re} = 1$), it can be seen that the flow rotation generated by the 3-D vortex at a higher Reynolds number enhances the species mixing considerably.

Figure 11 presents the experimental flow images obtained for the evolution of the flow rotation in the circular micro-chamber mixer with Rhodamine B fluorescence dye and containing blue dye, respectively, at a Reynolds number of $\text{Re} = 3$. It can be seen that the “sufficiently large” inertia forces existing in the flow at this Reynolds number cause the gradual evolution of a flow rotation in the circular micro-chamber. The experimental results are in good agreement with the numerical predictions.

Finally, Fig. 12 presents the optimized operating conditions for the current unbalanced driving force circular microfluidic mixer under Reynolds numbers ranging from $\text{Re} = 0.5$ to $\text{Re} = 6$. The optimal mixing ratio is found to be greater than 90% for the current flow conditions. Hence, the feasibility of the proposed unbalanced driving force circular microfluidic micromixer is confirmed.

Fig. 11 Experimental flow images of flow rotation in circular micro-chamber mixer at $\text{Re} = 3$ with different samples, (a) Rhodamine B, and (b) containing blue dye

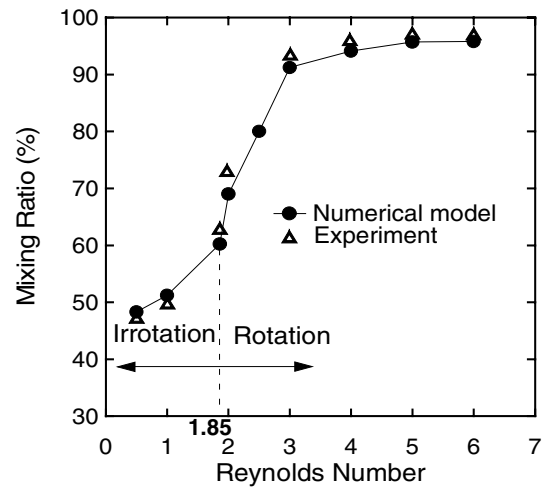
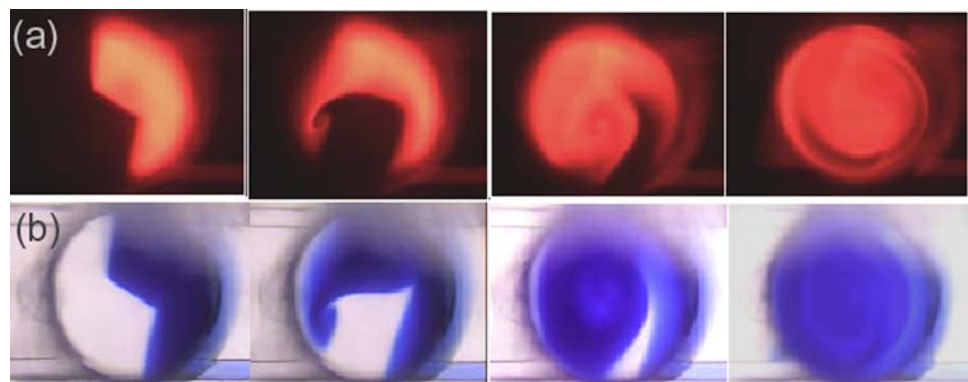


Fig. 12 Numerical calculations of mixing ratio at different Reynolds numbers

5 Conclusions

This study has developed a 3-D vortex passive micromixer utilizing an unbalanced driving force to perform efficient species mixing in a circular micro-chamber. The microfluidic mixer has a three-layered glass structure and is fabricated using a simple and reliable fabrication process. A numerical model has been developed to analyze the 3-D vortex streamline distribution and mixing performance. It has been shown that the numerical results are in good agreement with the experimental findings. When the Reynolds number exceeds a critical value of $\text{Re} = 1.85$, the streamline distribution in the circular micro-chamber transits from irrotational flow to rotational flow and produces a 3-D vortex. The mixing ratio obtained from irrotational flow is less than 65% at a cross-section located 100 μm downstream from the micro-chamber and is therefore insufficient to meet the mixing requirements of many applications. However, in rotational flow at a Reynolds number of $\text{Re} = 3$, the mixing ratio is enhanced to 91%. The unbalanced driving force circular microfluidic micromixer and numerical method presented in

this study provide a valuable contribution to the ongoing development of integrated microfluidic chips with an enhanced mixing performance.

Acknowledgments The current authors gratefully acknowledge the financial support provided to this study by the National Science Council of Taiwan under Grant Nos. NSC 94-2320-B-110-003 and NSC 94-2320-B-020-001. The authors would also like to thank Mr. Yue-Fung Lin for his kind assistance during the experimental stages of this study.

References

- E. Biddiss, D. Erickson, and D. Li, *Anal. Chem.* **76**, 3208 (2004).
 B.J. Burke and F.E. Regnier, *Anal. Chem.* **75**, 1786 (2003).
 C.C. Chang and R.J. Yang, *J. Micromech. Microeng.* **14**, 550 (2004).
 H. Chen and J.C. Meiners, *Appl. Phys. Lett.* **84**, 2193 (2004).
 Y.C. Chung, Y.L. Hsu, C.P. Jen, M.C. Lu, and Y.C. Lin, *Lab on a Chip* **4**, 70 (2004).
 J.T. Coleman and D. Sinton, *Microfluidics Nanofluidics* **1**, 319 (2005).
 A. Dodge, M.C. Jullien, Y.K. Lee, X. Niu, F. Okkels, and P. Tabeling, *Comptes Rendus Physique* **5**, 559 (2004).
 D. Erickson and D. Li, *Langmuir* **18**, 1883 (2002).
 R. Ferrigno, J.N. Lee, X. Jiang, and G.M. Whitesides, *Anal. Chem.* **76**, 2273 (2004).
 L.M. Fu and C.H. Lin, *Anal. Chem.* **75**, 5790 (2003).
 L.M. Fu, R.J. Yang, G.B. Lee, and Y.J. Pan, *Electrophoresis* **24**, 3026 (2003a).
 L.M. Fu, R.J. Yang, C.H. Lin, G.B. Lee, and Y.J. Pan, *Anal. Chimica ACTA* **507**, 163 (2004).
 L.M. Fu, R.J. Yang, C.H. Lin, and Y.S. Chien, *Electrophoresis* **26**, 1814 (2005).
 L.M. Fu and C.H. Lin, *Electrophoresis* **25**, 3652 (2005).
 T. Fujii, Y. Sando, K. Higashino, and Y. Fujii, *Lab on a Chip* **3**, 193 (2003).
 I. Glasgow, S. Lieber, and N. Aubry, *Anal. Chem.* **76**, 4825 (2004).
 S. Hardt and F. Schönfeld, *AIChE J.* **49**, 578 (2003).
 B. He, B.J. Burke, X. Zhang, R. Zhang, and F.E. Regnier, *Anal. Chem.* **73**, 1942 (2001).
 C.C. Hong, J.W. Choi, and C.H. Ahn, *Lab on a Chip* **4**, 109 (2004).
 F. Jiang, K.S. Drese, S. Hardt, M. Küpper, and F. Schönfeld, *AIChE J.* **50**, 2297 (2004).
 T.J. Johnson, D. Ross, and L.E. Locascio, *Anal. Chem.* **74**, 45 (2002).
 M. Kakuta, F.G. Bessoth, and A. Manz, *Chem. Rec.* **1**, 395 (2001).
 T.G. Kang and T.H. Kwon, *J. Micromech. Microeng.* **14**, 891 (2004).
 T. Kamei, N.M. Toriello, E.T. Lagally, R.G. Blazej, J.R. Scherer, R.A. Street, and R.A. Mathies, *Biomed. Microdevices* **7**(2), 147 (2005).
 D.S. Kim, S.W. Lee, T.H. Kwon, and S.S. Lee, *J. Micromech. Microeng.* **14**, 798 (2004a).
 D.S. Kim, I.H. Lee, T.H. Kwon, and D. Cho, *J. Micromech. Microeng.* **14**, 1294 (2004b).
 J.B. Knight, A. Vishwanath, J.P. Brody, and R.H. Austin, *Phys. Rev. Lett.* **80**, 3863 (1998).
 B.P. Leonard, *Proc. Int. Conf. on Numerical Methods in Laminar and Turbulent Flow, Part 1* (Pineridge Press, Swansea, 1987).
 C.H. Lin, L.M. Fu, and Y.S. Chien, *Anal. Chem.* **76**, 5265 (2004).
 C.H. Lin, C.H. Tsai, and L.M. Fu, *J. Micromech. Micromachining* **15**, 935 (2005).
 Y.Z. Liu, B.J. Kim, and H.J. Sung, *Int. J. Heat Fluid Fl.* **25**, 986 (2004).
 R.H. Liu, M.A. Stremmer, K.V. Sharp, M.G. Olsen, J.G. Santiago, R.J. Adrian, H. Aref, and D.J. Beebe, *J. Microelectromech. S.* **9**, 190 (2000).
 R.H. Liu, R. Lenigk, R.L. Druyor-Sanchez, J. Yang, and P. Grodzinski, *Anal. Chem.* **75**, 1911 (2003).
 P. Löb, K.S. Drese, V. Hessel, S. Hardt, C. Hofmann, H. Löwe, R. Schenk, and F. Schönfeld *Chem. Eng. Technol.* **27**, 340 (2004).
 H. Mao, T. Yang, and P.S. Crèmer, *J. Am. Chem. Soc.* **124**, 4432 (2002).
 V. Mengeaud, J. Josserand, and H.H. Girault, *Anal. Chem.* **74**, 4279 (2002).
 X. Niu, and Y.K. Lee, *J. Micromech. Micromachining* **13**, 454 (2003).
 S.J. Park, J.K. Kim, J. Park, S. Chung, C. Chung, and J.K. Chang, *J. Micromech. Microeng.* **14**, 6 (2004).
 F. Schönfeld, and S. Hardt, *AIChE J.* **50**, 771 (2004).
 A.D. Stroock, S.K.W. Dertinger, A. Ajdari, I. Mezić, H.A. Stone, and G.M. Whitesides, *Science* **295**, 647 (2002).
 Z. Tang, S. Hong, D. Djukic, V. Modi, A. West, J. Yardley, and R.M. Osgood, *J. Micromech. Microeng.* **12**, 870 (2002).
 M. Tabuchi, M. Ueda, N. Kaji, Y. Yamasaki, Y. Nagasaki, K. Yoshikawa, K. Kataoka, and Y. Baba, *Nat. Biotechnol.* **22**, 337 (2004).
 J.P. van Doormal and G.D. Raithby, *Numer. Heat Transfer* **7**, 147 (1984).
 R.A. Vijayarangan, K.M. Motsegood, D.J. Beebe, and D.E. Leckband, *Langmuir* **19**, 1824 (2003).
 K. Wang, S. Yue, L. Wang, A. Jin, C. Gu, P. Wang, Y. Feng, Y. Wang, and H. Niu, *Microfluidics Nanofluidics* **2**, 85 (2006).
 C.W. Wei, J.Y. Cheng, and T.H. Young, *Biomed. Microdevices* **8**, 65 (2006).
 S.H. Wong, M.C.L. Ward, and C.W. Wharton, *Sensor. Actuator. B.* **100**, 365 (2004).
 Z. Wu, N.T. Nguyen, and X.Y. Huang, *J. Micromech. Microeng.* **14**, 604 (2004).
 Z. Wu and N.T. Nguyen, *Biomed. Microdevices* **7**(1), 131 (2005).
 Q. Xiang, B. Xu, R. Fu, and D. Li, *Biomed. Microdevices* **7**(4), 273 (2005).
 X. Xuan and D. Li, *Electrophoresis* **26**, 3552 (2005).
 Z. Yang, H. Goto, M. Matsumoto, and R. Maeda, *Electrophoresis* **21**, 116 (2000).
 G.G. Yaralioglu, I.O. Wygant, T.C. Marentis, and B.T. Khuri-Yakub, *Anal. Chem.* **76**, 3694 (2004).